

Resources has developed a two-level land use classification system (12/73 categories); the European Union’s CORINE employs a three-level structure (5/15/44 categories); and the UK Environment Agency implements a four-level hierarchy (15/78/150/600 categories). Flattened methods struggle to generate semantically consistent and structurally aligned hierarchical classification results in an end-to-end pipeline, making them difficult to adapt to the aforementioned multi-level interpretation requirements. Furthermore, different application scenarios demand varying levels of interpretation granularity. For instance, natural resource monitoring may only require the identification of Artificial surfaces, while urban-rural land classification necessitates further subdivision of residential, industrial, and transportation facilities, demanding models with multi-granularity hierarchical interpretation capabilities.

2) Classification system differences hinder cross-domain generalization. In addition to the differences in general LCLU classification systems, various domains have also developed dedicated classification standards based on their specific needs. For example, the National Forestry and Grassland Administration of China employs a two-level hierarchy for forest land (8 primary categories and 13 subcategories), while the Ministry of Housing and Urban-Rural Development has established a three-level system for urban land use (8, 35, and 44 categories, respectively). Due to discrepancies in category definitions, semantic granularity, and hierarchical structures, existing LCLU models often encounter significant classification biases when directly transferred to tasks in other domains. Furthermore, most current models lack the ability to adaptively extend category hierarchies. For instance, in crop classification tasks, cropland needs to be further subdivided by crop type. However, existing approaches typically require retraining the entire model to accommodate new classification requirements and heavily rely on large amounts of annotated data. In practice, domain-specific applications often suffer from limited labeled samples, which further restricts the generalizability and real-world applicability of these models.

To achieve hierarchical LCLU results, several studies have attempted to incorporate the hierarchical category information into model design [10]–[12]. However, most of these methods rely on specific model architectures, making them incompatible with various modern network designs and unable to fully leverage high-performing foundation models recently introduced in the RS community (e.g., SkySense [13], RingMo [14], HyperSIGMA [15]). Additionally, the adaptability of these methods to multi-modal RS data remains unverified, limiting their potential in complex real-world scenarios. Moreover, recent studies have begun to explore domain adaptation in LCLU tasks, aiming to mitigate domain shifts caused by variations in sensors and geographic regions [16]–[20]. Although these studies have achieved some progress, they still primarily concentrate on the LCLU task itself. There remains a lack of systematic investigation into how existing LCLU models can be effectively transferred to other EO tasks (e.g., crop classification, flood detection), which hinders their broader applicability and generalization across diverse EO applications.

To address the aforementioned challenges, this paper proposes HieraRS, a general-purpose hierarchical LCLU classification method for RS scenarios. It enables semantically consistent, multi-granularity information extraction and supports the efficient transfer of LCLU models to cross-domain tasks, thereby significantly expanding their application potential. Specifically, we introduce a Bidirectional Hierarchical Consistency Constraint Mechanism (BHCCM) that seamlessly embeds complex hierarchical category systems into existing flat classification methods, enabling the model to acquire powerful multi-granularity interpretation capabilities. To support effective transfer of LCLU models to diverse cross-domain tasks, we present TransLU, a novel cross-domain transfer framework. TransLU establishes semantic correlations between LCLU tasks and novel tasks by leveraging a cross-domain tree-structured hierarchy. By integrating Cross-Domain Knowledge Sharing (CDKS) and Cross-Domain Semantic Alignment (CDSA) strategies, it supports dynamic category expansion, allowing for flexible adaptation of new classification requirements, and significantly enhances the adaptability of LCLU models across diverse scenarios.

Additionally, to comprehensively evaluate the effectiveness of the proposed HieraRS, we construct MM-5B, a large-scale, multi-modal hierarchical land use dataset. The MM-5B dataset includes data from three distinct sensor types with varying spectral configurations and spatial resolutions, and provides fine-grained pixel-level annotations across three hierarchical levels, containing 4, 9, and 18 classes, respectively, totaling 31 categories with varying semantic granularity.

The contributions of this paper are summarized as follows:

- 1) We construct MM-5B, a multi-modal hierarchical land use dataset that serves as a new benchmark for evaluating both hierarchical and multi-modal LCLU classification methods.
- 2) We introduce BHCCM, a bidirectional hierarchical consistency constraint mechanism that can be seamlessly integrated into mainstream flat methods to achieve multi-granularity hierarchical interpretation, while simultaneously improving prediction consistency and classification accuracy.
- 3) We propose TransLU, a cross-domain transfer framework that integrates CDKS and CDSA. TransLU supports dynamic category expansion and enables the efficient transfer of LCLU models to cross-domain tasks with heterogeneous classification systems.
- 4) We introduce a hierarchical semantic consistency loss function (\mathcal{L}_{HSC}) to regularize the overall training process and enforce strict semantic consistency across predictions at all hierarchical levels.

The remainder of this paper is organized as follows: Section II reviews representative LCLU classification datasets and related work. Section III describes the construction of the proposed MM-5B dataset. Section IV details the proposed methodology and key technical components. Section V presents the experimental setup and results. Finally, Section VI concludes the paper and outlines future directions.

II. RELATED WORK

In this section, we first introduce several representative datasets for land cover and land use classification. We then review key methodologies in the field of RS for hierarchical LCLU classification. Finally, we discuss the major challenges associated with cross-domain transfer in current LCLU approaches.

A. Pixel-level Annotated LCLU Classification Datasets

Pixel-level LCLU classification aims to assign a corresponding category label to each pixel in RS imagery. To facilitate automated analysis of large-scale RS data, the RS community has developed numerous LCLU datasets to support the training of machine learning and DL models. Table I provides an overview of 12 representative LCLU datasets, covering various spatial resolutions and sensor types, including RGB [21]–[23], MSI [3], [24], HSI [25], and multi-modal combinations [26], [27]. These datasets encompass both urban and rural environments and include annotated categories such as buildings, roads, impervious surfaces, cultivated land, and forest land.

However, as observed in Table I, existing LCLU datasets still exhibit several limitations, including single-modality design, limited diversity in spatial resolution, restricted category variety, and coarse annotation granularity. These constraints hinder a comprehensive evaluation of the proposed HieraRS under cross-domain and multi-source conditions. To address this gap, we extend the fine-grained annotations from the Five-Billion-Pixels dataset [3] by incorporating additional imagery from Google Earth and Sentinel-2, thereby constructing the Multi-modal Five-Billion-Pixels (MM-5B) dataset—a large-scale, multi-modal, hierarchical land use benchmark. MM-5B comprises 136 scenes, each associated with three distinct sensor (Google, Sentinel-2, and GaoFen-2) offering varying spatial resolutions (1 m, 4 m, and 10 m) and spectral configurations (3-band, 4-band, and 10-band), and provides fine-grained, pixel-level annotations across three hierarchical levels, with 4, 9, and 18 classes respectively, totaling 31 semantically diverse categories.

B. Hierarchical Land Cover and Land Use Classification

In the field of RS, DL-based LCLU classification is typically formulated as a semantic segmentation task [3], [32]–[38]. Most existing methods adopt a flat classification paradigm, where all classes are treated as mutually exclusive and independent, thereby ignoring the inherent hierarchical relationships among categories. This assumption contradicts the tree-structured classification systems widely employed in practical EO applications. While coarse-level predictions can be obtained by aggregating results from finer levels, this approach heavily depends on the accuracy of fine-grained classification. Errors at lower levels tend to propagate upward through the hierarchy, leading to cumulative deviations in higher-level semantic predictions [11]. Consequently, the flat classification paradigm suffers from limited generalization ability and reduced applicability in real-world EO scenarios.

TABLE I
COMPARISON OF PIXEL-LEVEL ANNOTATED DATASETS FOR LAND COVER AND LAND USE CLASSIFICATION DATASETS

Dataset Name	Classes	Modality	Resolution
LoveDA [21]	7	RGB	0.3 m
GAMUS [28]	6	RGB, nDSM	0.33 m
DeepGlobe [23]	7	RGB	0.5 m
Chesapeake [24]	6	RGB, MSI	2 m
WHDL [22]	6	RGB	2 m
BDCI2020 [29]	7	RGB	2 m
GID [30]	15	RGB, NIR	4 m
Five-Billion-Pixels [3]	24	RGB, MSI	4 m
SEN12MS [26]	17	Sentinel-1/2	10 m
DFC2020 [27]	10	Sentinel-1/2	10 m
WHU-OHS [25]	24	HSI	10 m
OpenSentinelMap [31]	15	RGB, Sentinel-2	10 ~ 60 m
MM-5B (our)	4 / 9 / 18 (31 total)	RGB (1 m, 3 band) MSI (4 m, 4 band) MSI (10 m, 10 band)	1 / 4 / 10 m

To address the above challenges, recent studies have begun to explore hierarchical LCLU classification methods. Adam et al. [39] demonstrated through experiments on Sentinel-2 time-series data that hierarchical classification outperforms traditional flat approaches in complex land cover recognition. To more effectively model hierarchical relationships among categories, Yang et al. [10] introduced class hierarchies derived from geospatial databases, and proposed a joint optimization strategy [40] to enhance hierarchical prediction consistency. Hiera-UNet [11] introduced coarse-level predictions as soft constraints into fine-level classification to achieve hierarchical information transfer. Kang et al. [12] extended the hierarchical segmentation framework [41] by integrating attribute-based hierarchical structures and a decision-level fusion strategy, leading to improved classification accuracy. In addition, Liu et al. [42] proposed a data-driven clustering method that automatically constructs hierarchical classification systems, which achieved better performance than manually defined hierarchies.

These hierarchical LCLU methods have provided technical support for producing more fine-grained and semantically rich products. However, in modeling hierarchical structures, many of these approaches [10], [11] rely on specific architectural designs, limiting their compatibility with recently developed flat network architectures in hierarchical classification tasks. Moreover, existing studies generally lack a systematic investigation into their adaptability to multi-modal RS data. To address these challenges, we propose BHCCM, which can be seamlessly integrated into existing flat classification models to achieve end-to-end hierarchical LCLU classification. It supports multi-granularity predictions aligned with predefined tree-structured hierarchies while simultaneously improves both prediction consistency and classification accuracy.

C. Cross-domain Transfer of LCLU Classification Models

In recent years, extensive research has been devoted to cross-domain adaptation for LCLU classification in the RS field, primarily aiming to address domain shift issues caused by variations in sensors, datasets, geographic regions, and temporal contexts. However, most of these efforts remain

confined to the LCLU task itself [16]–[18], [18], [20], with limited exploration of transferring existing LCLU models to other EO tasks (e.g. crop classification and flood detection). This lack of generalization significantly hinders the reusability of LCLU models across diverse EO application scenarios.

To address this gap, we propose TransLU, a dual-branch cross-domain transfer framework designed to bridge LCLU classification with diverse EO tasks. TransLU enables the efficient transfer and reuse of hierarchical LCLU models across a broader range of applications. To the best of our knowledge, this is the first general framework that systematically investigates the transfer of LCLU models to other EO tasks based on hierarchical category structures, offering a novel research paradigm and technical route for cross-domain migration in intelligent RS interpretation. In the experimental evaluation, we systematically assess TransLU on representative tasks, including crop classification and LCLU classification under varying hierarchical systems. The results demonstrate that TransLU exhibits strong adaptability and consistently outperforms baseline approaches across a variety of cross-domain EO scenarios.

III. MM-5B DATASETS

This section introduces the Multi-modal Five-Billion-Pixels (MM-5B) dataset, a large-scale multi-modal hierarchical land use dataset.

A. Workflow of Dataset Construction

The MM-5B dataset is an extension of the Five-Billion-Pixels dataset [3], constructed by incorporating additional imagery from Google Earth and Sentinel-2. It constitutes a multi-modal hierarchical land use dataset with varied spatial resolutions and spectral configurations. The original Five-Billion-Pixels dataset consists of 150 scenes of Gaofen-2 imagery covering regions across China, with a total coverage area of approximately 60,000 square kilometers. The Gaofen-2 imagery includes four spectral bands—blue (450–520 nm), green (520–590 nm), red (630–690 nm), and near-infrared (770–890 nm)—with a spatial resolution of 4 meters. In accordance with the *Land use classification standard of China (GB/T 21010-2017)* and the identifiable characteristics of 4 meter optical RS imagery, land cover was categorized into 24 distinct classes. Pixel-level annotations were performed by trained experts with domain knowledge.

The MM-5B dataset is constructed from multi-source satellite imagery collected from Google Earth, GaoFen-2, and Sentinel-2, each with distinct spatial resolutions and spectral configurations. Specifically, Google Earth imagery provides 1-meter resolution with three spectral bands (RGB); GaoFen-2 provides MSI with four bands (RGB and NIR) at a resolution of 4-meters; and Sentinel-2 imagery delivers 10-band MSI (B2–B8, B8A, B11, and B12) with a spatial resolution of 10 meters. These three data sources are complementary in both of spatial resolution and spectral information. This combination effectively supports a wide range of typical application scenarios in optical RS tasks and offers rich information for multi-modal analysis.

The dataset construction process is as follows: To achieve spatial alignment across multi-source imagery, we first performed geo-rectification on the GaoFen-2 images and their corresponding labels. Specifically, we applied rigorous geometric correction using the Rational Polynomial Coefficients (RPC) provided with the original dataset, combined with the Copernicus 30-meter resolution Digital Elevation Model (DEM) and 4-meter resolution Google Earth imagery as references data. All registration results were manually inspected and quality-checked to ensure spatial consistency. Subsequently, based on the geo-rectified Gaofen-2 regions, we collected imagery covering the same geographic areas and similar acquisition times from both the Google Earth and Sentinel-2 platforms. This resulted in 1-meter resolution RGB imagery from Google Earth and 10-meter resolution MSI from Sentinel-2. Finally, the geo-rectified 4-meter resolution labels were pixel-wise aligned with the 1-meter RGB and 10-meter MSI, forming the multi-modal land use dataset MM-5B composed of three data sources. Fig. 2 illustrates sample data from the MM-5B dataset, demonstrating the complementarity of spatial resolution and spectral characteristics across modalities.

B. Organization of the Tree-structured Hierarchy

In addition, we refined the original 24-class labels to 18 classes based on the interpretability of land cover types at a 10-meter spatial resolution. Specifically, irrigated field and dry cropland were merged into dry cropland; garden land, shrub forest, and arbor forest were grouped into forest; fish pond and pond were merged into pond; park and square were combined, and the glacier and snow category was removed due to seasonal inconsistencies in acquisition time. As a result, the final MM-5B dataset consists of 136 scenes, each containing multi-modal data from three sensor types and pixel-wise annotations across 18 land cover classes. Prior to public release, additional manual inspections will be conducted to ensure label quality. The dataset will be made publicly available at <https://github.com/AI-Tianlong/HieraRS>.

One of the key contributions of this paper is the introduction of BHCCM, which can be seamlessly integrated into flat classification methods to achieve hierarchical LCLU classification. In MM-5B, 18 land use categories are organized into a three-level hierarchy with increasing semantic granularity from L1 to L3. Specifically, L1 includes four broad classes: vegetation, water, artificial surfaces, and bare land; L2 refines them into nine intermediate classes; and L3 further divides them into 18 fine-grained categories. The tree-structured hierarchy is illustrated in Fig. 2. During model training, the dataset pipeline dynamically constructs hierarchical labels based on the predefined tree structure, without requiring any manual preprocessing of the hierarchical annotations.

The proposed MM-5B dataset can be used not only for training hierarchical LCLU classification models under single-source settings, but also serves as a novel multi-modal land use classification benchmark for the RS community. We believe that by leveraging the complementary information from high-resolution optical imagery and medium-resolution MSI, more

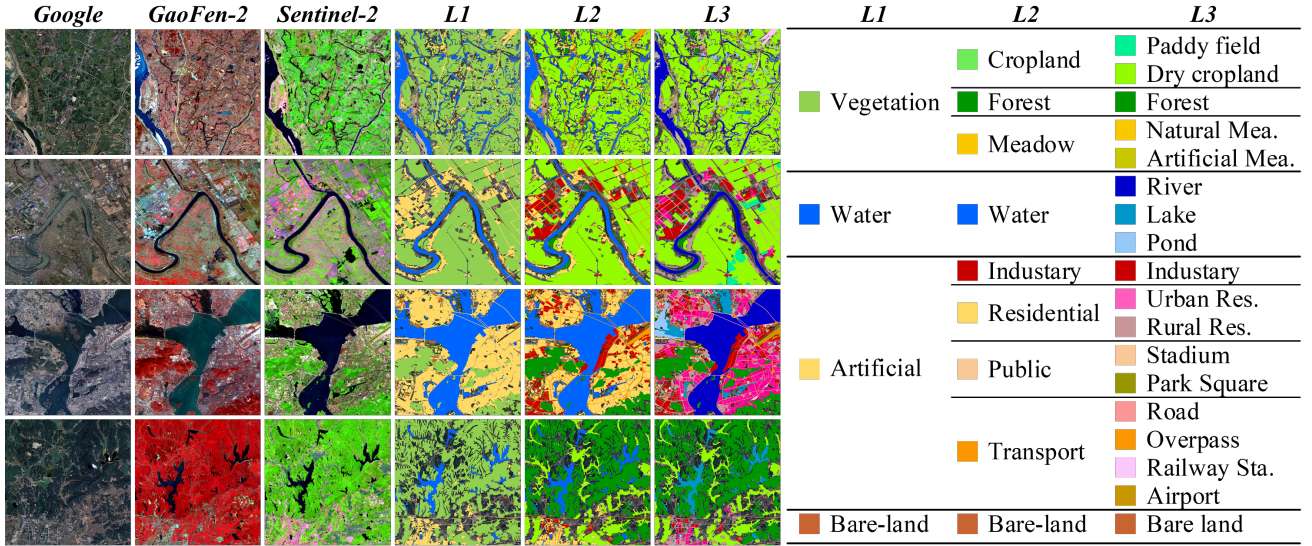


Fig. 2. Illustration of the MM-5B dataset. The left panel shows visualizations of three paired data sources and their corresponding labels at three hierarchical levels: Google Earth (RGB), GaoFen-2 (B4-B2-B1, false color), and Sentinel-2 (B12-B8A-B4, SWIR). The right panel presents the tree-structured hierarchical classification system of the MM-5B, consisting of three levels: L1 with 4 categories, L2 with 9 categories, and L3 with 18 categories.

accurate land use mapping can be achieved. We believe this research direction holds promising potential for advancing intelligent EO applications.

IV. METHODOLOGY

This section presents HierRS, a hierarchical segmentation paradigm tailored for RS-based EO applications. It is designed to support both multi-granularity interpretation and cross-domain task transfer.

A. Overview of the Proposed Method

This work targets two main objectives: i) to develop an independent mechanism that can be seamlessly integrated into existing flat classification methods to achieve multi-granularity hierarchical LCLU classification. ii) to design a generalizable framework for effectively transferring LCLU models to cross-domain EO tasks with heterogeneous classification systems. To this end, we introduce BHCCM and TransLU, each addressing one of the respective goals.

Figure 3 presents the overall architecture of the proposed approach. We define HierRS as a two-stage hierarchical interpretation paradigm composed of BHCCM and TransLU. It is designed to exploit the intrinsic hierarchical structure of land cover categories to enforce prediction consistency across levels and support transferability to cross-domain EO tasks.

In the first stage, our goal is to transform existing flat classification methods into hierarchical classification models capable of multi-granularity semantic consistency prediction. By training the proposed BHCCM on the MM-5B dataset, we can obtain a model capable of multi-granularity interpretation of basic ground object categories. The second stage is defined as the transfer process of the LCLU classification model. With the proposed TransLU framework and its two key components, CDKS and CDSA, the hierarchical LCLU model trained in the

first stage can be effectively transferred to new cross-domain tasks. Stage II in Fig. 3 presents an example of transferring the LCLU classification model to a crop classification task.

B. Bidirectional Hierarchical Consistency Constraint Mechanism

In Stage I, the proposed BHCCM can be seamlessly integrated into existing flat classification methods, transforming them into hierarchical LCLU models with semantically consistent multi-granularity predictions. Fig. 3 (a) illustrates the position and role of BHCCM in the overall structure. Fig. 4 provides a detailed view of the BHCCM architecture. The trapezoid labeled “Decoder” denotes the decoder design typical of flat semantic segmentation models such as UperNet [43] and DeepLabv3+ [44]. Conventionally, a 2D convolution is applied at the decoder’s output to project the upsampled features from $\mathbb{R}^{B \times C_{\text{dim}} \times H \times W}$ to $\mathbb{R}^{B \times C_{L_3} \times H \times W}$, yielding predictions for the finest level (L3) in the hierarchy.

In our proposed hierarchical method, the final layer is replaced by BHCCM to enable parallel prediction at three semantic levels (L1, L2, and L3). Specifically, BHCCM takes the decoder output and feeds it into three separate convolutional layers with different output channel sizes, generating initial prediction maps of shape $\mathbb{R}^{B \times C_{L_i} \times H \times W}$, where $C_{L_1} = 4$, $C_{L_2} = 9$, and $C_{L_3} = 18$, corresponding to the number of classes at the coarse-to-fine levels in the MM-5B dataset. These initial prediction features are denoted as F_{in}^i ($i = 1, 2, 3$).

BHCCM employs bidirectional semantic consistency constraints to enable effective cross-level interaction. In contrast to prior work [12], [41] that applies hierarchical loss in a passive manner, BHCCM explicitly encodes parent-child semantic dependencies and conducts two-way feature

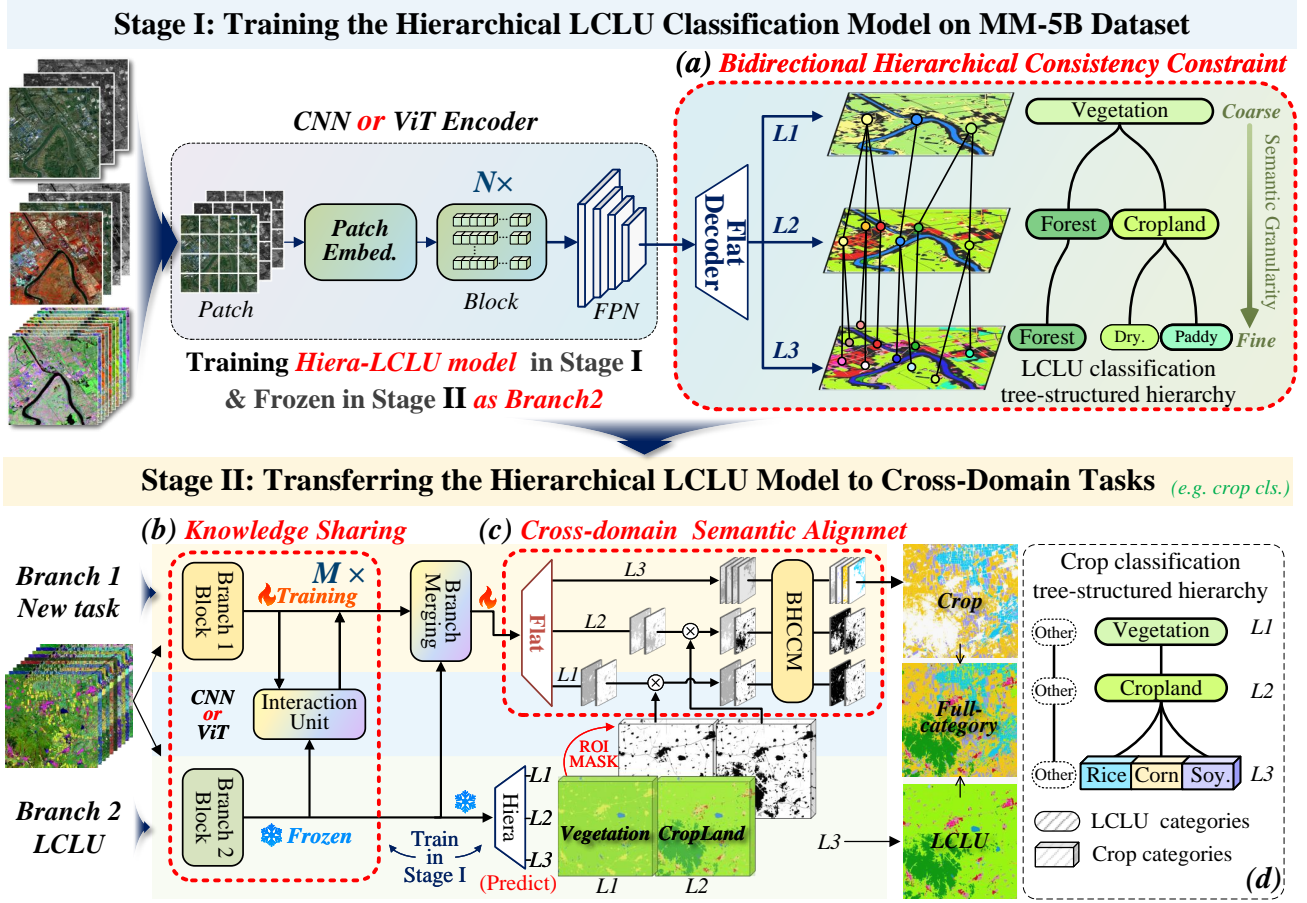


Fig. 3. Overview of the proposed HieraRS. In Stage I, (a) BHCCM seamlessly integrates into flat classification methods, transforming them into hierarchical LCLU classification models. Stage II represents the TransLU framework, designed to achieve cross-domain transfer of LCLU models. (b) illustrates CDKS, used for feature interaction and knowledge sharing in cross-domain tasks; (c) depicts CDSA, for cross-domain feature semantic alignment; and (d) shows the cross-domain tree-structured hierarchy used for transferring LCLU to crop classification tasks.

fusion—from coarse to fine and fine to coarse—as depicted by the green and blue arrows in Fig. 4. In the coarse-to-fine path (green arrows in Fig. 4), coarse-level semantic features are used to guide the refinement of fine-grained predictions. Taking L2 as an example, the intermediate feature F_{mid}^2 consists of two components: i) F_{in}^1 processed through a coarse-to-fine merging block (MB) and weighted by W_2^1 , and ii) F_{in}^2 weighted by W_2^2 . Similarly, F_{mid}^3 integrates information from L1, L2, and L3. This process can be formulated as:

$$F_{mid}^1 = F_{in}^1 \quad (1)$$

$$F_{mid}^2 = W_2^1 \cdot \text{MB}(F_{in}^1) + W_2^2 \cdot F_{in}^2 \quad (2)$$

$$F_{mid}^3 = W_3^1 \cdot \text{MB}(F_{in}^1) + W_3^2 \cdot \text{MB}(F_{in}^2) + W_3^3 \cdot F_{in}^3 \quad (3)$$

In the fine-to-coarse path (blue arrows in Fig. 4), the fused fine-level features at L3 form the final output F_{out}^3 , which is then used to guide the upper levels L2 and L1. Specifically, F_{out}^2 and F_{out}^1 are obtained by processing the corresponding intermediate features through fine-to-coarse MB, following the pathways indicated by the blue arrows. This process can be

formulated as:

$$F_{out}^1 = Y_1^3 \cdot \text{MB}(F_{mid}^3) + Y_1^2 \cdot \text{MB}(F_{mid}^2) + Y_1^1 \cdot F_{mid}^1 \quad (4)$$

$$F_{out}^2 = Y_2^3 \cdot \text{MB}(F_{mid}^3) + Y_2^2 \cdot F_{mid}^2 \quad (5)$$

$$F_{out}^3 = F_{mid}^3 \quad (6)$$

To enable effective information transfer across hierarchical levels, we design a Merging Block (MB) that incorporates both channel and spatial attention to produce intermediate features that are semantically guided and dimensionally aligned with the target level. As shown in Fig. 5, the channel attention branch applies global average pooling and max pooling to the input features, generating two vectors that are passed through a shared MLP and projected to the target-level dimensionality, producing a channel attention map. Simultaneously, spatial attention is obtained by performing channel-wise pooling, concatenation, convolution, and activation on the input features, resulting in a spatial attention map. Finally, the source-level features are element-wise multiplied with both attention maps to achieve semantic enhancement and dimensional alignment.

In summary, BHCCM serves two roles: in Stage I, it enables multi-granularity hierarchical LCLU prediction by integrating

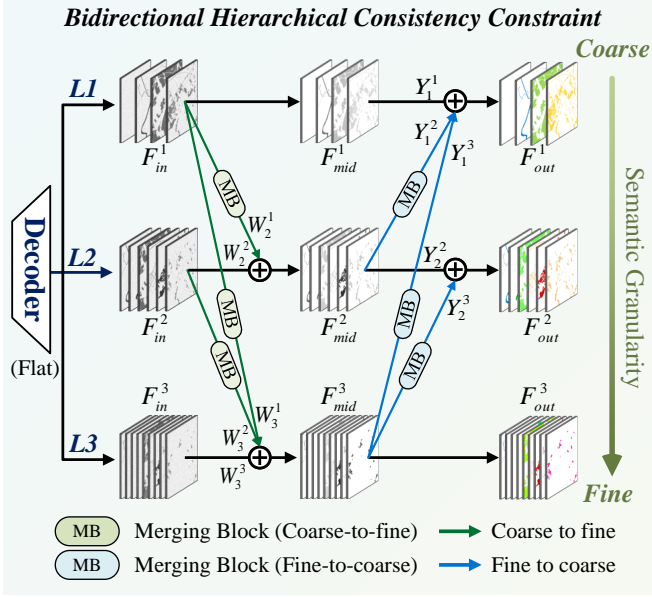


Fig. 4. Detailed structure of BHCCM. The figure illustrates the bidirectional information flow pathways, where semantic feature interaction and fusion across hierarchical levels are achieved via coarse-to-fine (green arrows) and fine-to-coarse (blue arrows) connections.

with flat classifiers; in Stage II, it is reused within the CDSA module of TransLU to facilitate cross-domain transfer of LCLU models.

C. Cross-domain Transfer Framework—TransLU

We propose TransLU, a novel dual-branch cross-domain transfer framework that enables the hierarchical LCLU model trained in Stage I to be efficiently transferred to cross-domain EO tasks. As illustrated in Stage II of Fig. 3, TransLU consists of two parallel branches. Branch 2 corresponds to the pretrained hierarchical LCLU model in Stage I, with its parameters kept frozen during the transfer process. Branch 1 shares the same architecture as Branch 2 but is fine-tuned on the target task with trainable parameters.

To achieve knowledge sharing and semantic alignment between the LCLU task and the target-domain task, we propose a Cross-Domain Knowledge Sharing (CDKS) strategy that facilitates cross-branch feature interaction between the two encoders. In addition, to fully exploit the strong representational capacity of the hierarchical LCLU model trained on large-scale data, we introduce a Cross-Domain Semantic Alignment (CDSA) strategy. CDSA employs a cross-domain tree-structured hierarchy, where multi-granularity predictions from the LCLU model are used to impose semantic constraints on the target branch, thereby enhancing the adaptability to new-domain tasks.

1) *Cross-domain Knowledge Sharing*: To promote faster convergence and superior performance in cross-domain transfer, we implemented weight sharing between the encoders of Branch 1 and Branch 2 within our dual-branch TransLU architecture. Moreover, to ensure Branch 1 continuously benefits from the robust representation capabilities learned by

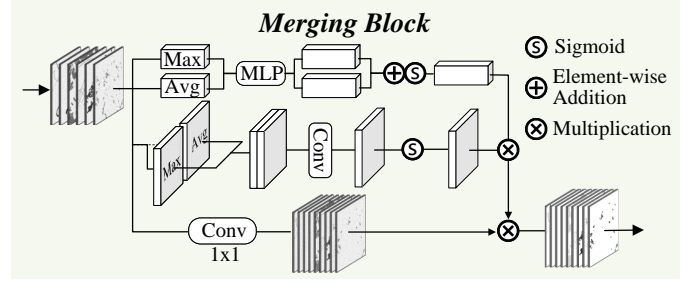


Fig. 5. Detailed Structure of the Merging Block. It consists of two feature extraction branches: a channel attention branch and a spatial attention branch.

Branch 2 during end-to-end training, and inspired by [45], we propose CDKS specifically for cross-domain task transfer. In the complete Encoder of TransLU, CDKS consists of multiple branch interaction units (BIUs), explicitly connecting the two branches for efficient information sharing and feature fusion between them. The detailed structure of a BIU is presented in Fig. 6.

In the specific implementation, we denote the outputs of the i -th encoder block from Branch 1 and Branch 2 as \mathcal{F}_1^i and \mathcal{F}_2^i , respectively. To establish effective information interaction between the two branches, we introduce deformable cross-attention [46], denoted as $\text{Attn}(\cdot)$. Since Branch 2 is frozen during training, only the features in Branch 1 are updated. Before the attention operation, a linear projection layer $\text{FC}(\cdot)$ is first applied to align the key and value dimensions from Branch 2 with the query from Branch 1. Deformable attention then extracts supplementary information from \mathcal{F}_2^i and integrates it into \mathcal{F}_1^i . To reinforce feature fusion, we apply a feed-forward network $\text{FFN}(\cdot)$ for channel-wise refinement. The feature sharing process for Branch 1 after the i -th block can be formulated as:

$$\hat{\mathcal{F}}_1^i = \mathcal{F}_1^i + \gamma_1^i \text{Attn}(\text{norm}(\mathcal{F}_1^i), \text{norm}(\text{FC}(\mathcal{F}_2^i))), \quad (7)$$

$$\tilde{\mathcal{F}}_1^i = \hat{\mathcal{F}}_1^i + \tau_1^i \text{FFN}(\text{norm}(\hat{\mathcal{F}}_1^i)). \quad (8)$$

where $\text{norm}(\cdot)$ refers to LayerNorm [47]. τ_1^i and γ_1^i are learnable parameters, and $\hat{\mathcal{F}}_1^i$ denotes the interaction output. Both τ_1^i and γ_1^i are initialized to zero to prevent significant alteration of the original feature distribution of \mathcal{F}_1^i during the interaction process, thereby better preserving the pretrained knowledge derived from LCLU classification tasks. This design establishes an asymmetric information flow between the two branches, allowing Branch 1 to continuously absorb the discriminative features encoded by Branch 2.

For CNN-based models such as ConvNeXt [48], after each feature interaction step, the features from Branch 1 and Branch 2 are fused via learnable weights W_1^i and W_2^i using a weighted sum. The fused features are then used as the input to the next block of Branch 1. In contrast, for Transformer-based models such as ViT [49], following the setup in [45], we perform M feature interaction steps ($M = 12$), and apply the weighted fusion only once at the final step. The resulting fused representation serves as the final feature of Branch 1. Branch 2 remains independent and outputs its final features directly from the last block, denoted as \mathcal{F}_2^M . The outputs from

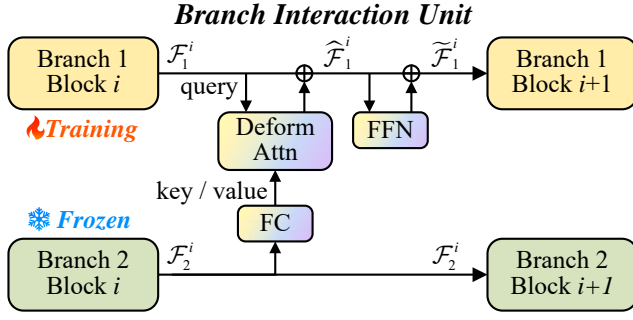


Fig. 6. Detailed structure of the branch interaction unit. It consists of a deformable cross-attention, a fully-connect layer, and a feed-forward network.

both branches are then fed into their respective BHCCM for hierarchical prediction.

2) *Cross-domain Semantic Alignment*: To achieve efficient transfer of hierarchical LCLU classification models to new domain tasks, we propose a CDSA strategy, as illustrated in Fig. 3 (c). The core principle of CDSA is to integrate the multi-granularity predictions of the LCLU model into cross-task semantic alignment supervision, effectively guiding the learning process of the new task model. This fully leverages the robust representation capability of the hierarchical LCLU model trained on large-scale datasets.

First, we construct a cross-domain tree-structured hierarchy based on the categorical relationships between the hierarchical LCLU classification task and the new task, serving as a bridge connecting the semantic systems of the two tasks, as illustrated in Fig. 3 (d). During training and inference, for the same input image, Branch 2 (the frozen LCLU model) outputs a multi-level interpretation result based on its original LCLU classification system. Simultaneously, Branch 1 (the new task model) generates a hierarchical output consistent with the cross-domain tree-structured hierarchy.

Since the two tasks share categories or exhibit semantic overlap at higher semantic levels (e.g., vegetation or cropland), we can impose a hierarchical consistency constraint on the output of Branch 1 using the high-level interpretation results from Branch 2. The proposed CDSA not only enhances semantic alignment between the two tasks, but also enables the model for the new domain to receive effective supervision from the LCLU model with strong representational capacity at the early stages of training, leading to faster convergence and improved performance. As illustrated in Fig. 3 (c), CDSA establishes inter-branch interaction between the two branches through shared high-level semantics, effectively improving the generalization capability of the model on the target task.

Taking the transfer to a crop classification task as an example, Fig. 3 (b–d) illustrates the complete process of adapting the hierarchical LCLU model to the target domain. We begin by constructing a cross-domain hierarchical structure based on prior domain knowledge, linking semantic levels as follows: Vegetation \rightarrow Cropland \rightarrow Rice, Maize, Soybean. In this hierarchy, Vegetation and Cropland correspond to the L1 and L2 categories in the original land use classification task, while Rice, Maize, and Soybean represent newly introduced

L3 categories specific to the crop classification task. Based on this semantic mapping, we establish a cross-domain hierarchical tree (Fig. 3 (d)) that bridges the label spaces between land use and crop classification tasks.

During training, TransLU first generates three-level LCLU feature maps F_{out}^{L1} , F_{out}^{L2} , and F_{out}^{L3} through Branch 2. Then, based on the cross-domain tree-structured hierarchy, the feature tensors corresponding to vegetation and cropland, $F_{out}^{L1:veg}$ and $F_{out}^{L2:crop}$, are extracted from F_{out}^{L1} and F_{out}^{L2} , respectively. These are then processed by a softmax operation to produce soft region of interest (ROI) masks, denoted as $F_{soft}^{L1:veg}$ and $F_{soft}^{L2:crop}$.

Subsequently, the multi-scale feature maps produced by the Branch 1 encoder are passed through the decoder structure illustrated in Fig. 3 (c), generating three levels of initial input features, denoted as Z_{in}^{L1} , Z_{in}^{L2} , and Z_{in}^{L3} . The previously generated soft ROI masks are then incorporated into $Z_{in}^{L1:veg}$ and $Z_{in}^{L2:crop}$ through a weighted fusion strategy, resulting in enhanced feature representations \tilde{Z}_{in}^{L1} and \tilde{Z}_{in}^{L2} . These enriched features, along with Z_{in}^{L3} , are subsequently fed into the BHCCM of Branch 1 for cross-level interaction and final hierarchical prediction. For Branch 1, the inputs to the BHCCM at levels L1, L2, and L3, denoted as \tilde{Z}_{in}^{L1} , \tilde{Z}_{in}^{L2} , and \tilde{Z}_{in}^{L3} respectively, are defined as follows:

$$\tilde{Z}_{in}^{L1:veg} = Z_{in}^{L1:veg} \cdot F_{soft}^{L1:veg} \quad (9)$$

$$\tilde{Z}_{in}^{L2:crop} = Z_{in}^{L2:crop} \cdot F_{soft}^{L2:crop} \quad (10)$$

$$\tilde{Z}_{in}^{L1} = \left[Z_{in}^{L1:other}, \tilde{Z}_{in}^{L1:veg} \right] \quad (11)$$

$$\tilde{Z}_{in}^{L2} = \left[Z_{in}^{L2:other}, \tilde{Z}_{in}^{L2:crop} \right] \quad (12)$$

$$\tilde{Z}_{in}^{L3} = Z_{in}^{L3} \quad (13)$$

D. Hierarchical Semantic Consistency Loss Function

In BHCCM, although the bidirectional semantic consistency constraints can significantly enhance information interaction across hierarchical levels, they still cannot strictly guarantee pixel-wise semantic consistency across levels. To address this limitation, we further propose a hierarchical semantic consistency loss function (\mathcal{L}_{HSC}) and a joint scoring-bases path selection (JSPS) post-processing strategy. These components ensure strict semantic structural consistency across all levels in the model’s output, thereby enabling multi-granularity hierarchical predictions aligned with the predefined tree-structured hierarchy.

For conventional flat LCLU classification models, pixel-wise cross-entropy loss is typically employed to supervise the classification scores for each category. Its standard formulation is given as:

$$\mathcal{L}_{CE} = -\frac{1}{N} \sum_{n=1}^N \sum_{c=1}^C \hat{y}^{(c)} \log p^{(c)} \quad (13)$$

where N denotes the number of pixels in the image, C is the total number of categories, $\hat{y}^{(c)}$ is the one-hot encoded ground-truth label for class c , and $p^{(c)}$ is the predicted probability for that class.

This loss function has been widely used in conventional flat classification settings. However, in tasks with hierarchical structures, applying independent $\mathcal{L}_{\text{CE}}^{(L_i)}$ to each level cannot explicitly constrain semantic consistency across levels. To address this issue, we propose \mathcal{L}_{HSC} as a unified training objective for both BHCCM and TransLU. The loss \mathcal{L}_{HSC} consists of two components: the hierarchical cross-entropy loss \mathcal{L}_{HCE} and the hierarchical path consistency constraint \mathcal{L}_{HPC} . First, for the three output features F_{out}^i ($i = 1, 2, 3$) generated by BHCCM, we apply three separate cross-entropy losses to supervise each level individually. These losses are then jointly weighted to form the hierarchical cross-entropy loss \mathcal{L}_{HCE} , as follows:

$$\mathcal{L}_{\text{CE}}^{(L_i)} = -\frac{1}{N} \sum_{n=1}^N \sum_{i=1}^{C_{L_i}} y_{Li}^{(c)} \log p_{Li}^{(c)} \quad (14)$$

$$\mathcal{L}_{\text{HCE}} = \sum_{i=1}^3 \lambda_i \mathcal{L}_{\text{CE}}^{(L_i)} \quad (15)$$

where N denotes the total number of pixels in the image, C_{L_i} is the number of categories at the i -th hierarchical level, $y_{Li}^{(c)}$ is the one-hot encoded ground-truth label for pixel j and class c , and $p_{Li}^{(c)}$ denotes the predicted probability for that class at level i , λ_i is a weighting hyperparameter used to balance the losses across hierarchical levels. By default, all weights are set to $\lambda_i = 1$.

Secondly, we propose a hierarchical path consistency constraint loss function \mathcal{L}_{HPC} to explicitly supervise the semantic path structure across multiple hierarchical levels. Specifically, for each pixel i , let the model predictions at levels L1, L2, and L3 be denoted as y_1 , y_2 , and y_3 , respectively. We concatenate them to form a joint prediction vector: $Y_i = [y_1, y_2, y_3]$. Similarly, let \hat{y}_1 , \hat{y}_2 , and \hat{y}_3 be the one-hot encoded ground truth vectors at each level. The concatenated ground truth vector is: $\hat{Y}_i = [\hat{y}_1, \hat{y}_2, \hat{y}_3]$. We apply a log-softmax to the concatenated prediction vector Y_i to obtain the normalized log-probability distribution $\log P_i$. The Kullback–Leibler (KL) divergence between $\log P_i$ and the corresponding hierarchical label \hat{Y}_i is then computed to define the hierarchical path consistency loss \mathcal{L}_{HPC} as follows:

$$\mathcal{L}_{\text{HPC}} = \frac{1}{N} \sum_{i=1}^N \text{KL} \left(\log \text{Softmax}(Y_i), \hat{Y}_i \right) \quad (16)$$

where N is the number of pixels, \hat{Y}_i denotes the one-hot encoded ground-truth hierarchical path for pixel i , and $\log \text{Softmax}(Y_i)$ represents the predicted log-probability distribution over the valid semantic paths.

The final training loss is defined as a weighted combination of the \mathcal{L}_{HCE} and \mathcal{L}_{HPC}

$$\mathcal{L}_{\text{HSC}} = \mathcal{L}_{\text{HCE}} + \alpha \mathcal{L}_{\text{HPC}} \quad (17)$$

where α is a hyperparameter that balances the \mathcal{L}_{HCE} and \mathcal{L}_{HPC} . This joint loss formulation effectively promotes semantic coordination across levels, mitigates hierarchical conflicts in predictions, and ensures structurally coherent segmentation outputs.

Furthermore, to strictly enforce prediction consistency during inference, we propose a joint scoring-bases path selection (JSPS) post-processing strategy. Specifically, we compute the joint score for each valid path in the hierarchical structure and select the one with the highest joint score as the final multi-level prediction for each pixel, which can be formulated as:

$$\hat{y}_i = \arg \max_{y \in \mathcal{T}} \sum_{l=1}^L \sigma \left(s_i^{(l)} \right) \quad (18)$$

where \hat{y}_i denotes the predicted hierarchical label path for pixel i ; \mathcal{T} is the set of all valid hierarchical paths defined by the tree-structured classification system; L is the total number of semantic levels; $s_i^{(l)}$ denotes the logit score corresponding to class $y^{(l)}$ at level l for pixel i ; $\sigma(\cdot)$ is the sigmoid function.

By integrating the hierarchical semantic consistency loss \mathcal{L}_{HSC} during training and applying the proposed path selection post-processing strategy, our method produces multi-level LCLU classification results that are semantically coherent and structurally consistent across all hierarchical levels.

V. EXPERIMENTS

In this section, we present comprehensive experiments on three benchmark datasets to validate the effectiveness of the proposed HierRS.

A. Datasets

1) **MM-5B**: To evaluate the adaptability of the proposed BHCCM to multi-source RS data, we conduct hierarchical land use classification experiments on the MM-5B. A total of 107 images are used for training and 29 for validation. Sentinel-2 and GaoFen-2 images are cropped into non-overlapping patches of 512 and 640 pixels, respectively. To reduce training costs, the 1-meter Google Earth imagery is downsampled to 2 meters and cropped into patches of size 896×896 . The resulting training sets contain 2,370 samples for Sentinel-2, 15,091 for GaoFen-2, and 28,679 for Google Earth. The validation sets contain 632, 4,110, and 7,635 samples, respectively. All annotations follow a three-level hierarchical classification system, comprising 4 categories at L1, 9 at L2, and 18 at L3, as illustrated in Fig. 3.

2) **Crop10m**: To validate the effectiveness of the proposed TransLU, a cross-domain scenario is designed to transfer from hierarchical land use classification to crop classification. The annual crop classification product proposed by You et al. [50] is adopted as the ground-truth labels. Sentinel-2 imagery (10 m resolution, 10 spectral bands) over selected regions in Heilongjiang Province, China, is collected for rice, maize, and soybean classification experiments. The study area is illustrated in Fig. 7, with white- and red-bordered regions indicating the training and validation areas, respectively. The images are cropped into 512×512 patches, resulting in 678 training samples and 296 validation samples. The cross-domain hierarchical structure is illustrated in Fig. 3 (d).

3) **WHDL**: This dataset contains six valid annotated classes and is used to demonstrate how TransLU facilitates

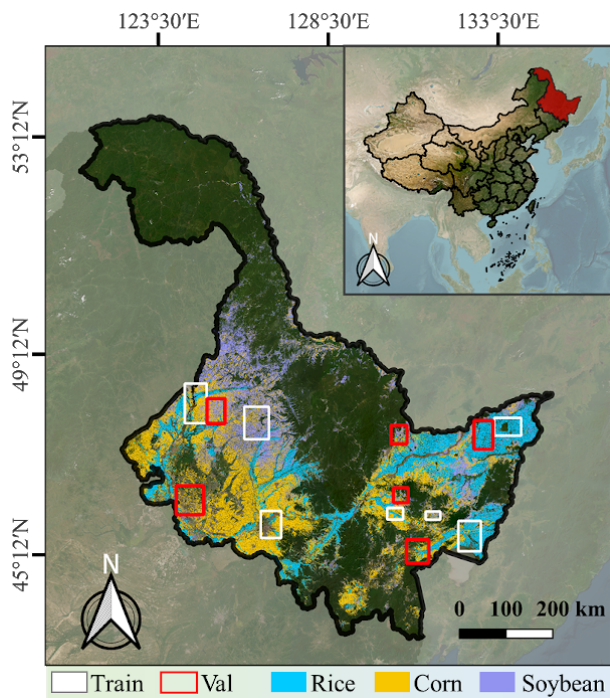


Fig. 7. Illustration of the study area in the Crop10m dataset. The study area is located in Heilongjiang Province, northeastern China. The dataset includes three valid crop categories: rice, corn, soybean. The white bounding box indicates the training region, while the red bounding box marks the validation region.

the adaptation of a pretrained LCLU model to a different tree-structured hierarchy. WHDL D comprises 4,940 RGB images, each with a size of 256×256 . Following a 2:1 split, we obtain 3,294 training samples and 1,646 validation samples. As illustrated in Fig. 11, the categories are organized into a two-level hierarchical structure.

B. Experimental Setup

To evaluate the compatibility of the proposed BHCCM with different model architectures, we conduct experiments on the MM-5B dataset using both CNN- and Transformer-based frameworks. We compare the performance of each model under a flat classification baseline and the hierarchical classification setup enabled by BHCCM. Specifically, DeepLabv3+ adopts ResNet-101 [51] as its backbone and is optimized using SGD, while ConvNeXt [48], SegNext [52], DeiT3 [53], and Swin [54] are trained using the AdamW optimizer. Performance is evaluated using mean Intersection over Union (mIoU) and mean Accuracy (mAcc). All models are trained for 80k iterations on each of the three data modalities, implemented with the MMSegmentation framework [55], and executed on four NVIDIA A800 GPUs.

For the cross-domain transfer experiments on Crop10m and WHDL D, all experimental settings follow those of the MM-5B experiments, except that the number of training iterations is reduced to 20k.

C. Hierarchical LCLU Classification on MM-5B

1) *Quantitative Results*: Tables II, III, and IV present the hierarchical land use classification results on the three individual data sources of the MM-5B dataset. The results compare model performance with and without the integration of the proposed BHCCM, models incorporating BHCCM are shown in bold and marked with “(Hiera)”. For flat classification models that do not natively support multi-level outputs, L3 predictions are aggregated to L2 and L1 levels based on the tree-structured hierarchy defined in Fig. 2, and the corresponding mIoU and mAcc scores are computed accordingly.

As shown in the overall results of Table II, incorporating BHCCM into various models not only enables end-to-end hierarchical LCLU classification, but also consistently improves classification accuracy over the baseline models across all three hierarchical levels. Specifically, for the representative CNN-based model DeepLabv3+, integrating BHCCM yields mIoU improvements of 1.80%, 1.11%, and 0.51% at the L1, L2, and L3, respectively, along with corresponding mAcc gains of 0.21%, 0.43%, and 0.15%. Similarly, on the ConvNeXt architecture, BHCCM delivers stable gains, improving mIoU by 1.04%, 0.97%, and 0.54%, and mAcc by 1.09%, 1.10%, and 0.55% across the three levels. For the efficient and lightweight SegNeXt model, it is noteworthy that SegNeXt-S + BHCCM achieves an L3 mAcc of 74.77, surpassing even the SegNeXt-B flat baseline (74.74%), highlighting the efficacy of BHCCM in enhancing lightweight models without increasing backbone complexity. A similar trend is observed in the Transformer-based models. Swin-L with BHCCM achieves the best L3 mAcc (76.66%) among all models in this comparison. Moreover, mIoU improvements across the three hierarchical levels are observed: 0.46%, 0.78%, and 0.39%. Notably, Swin-B with BHCCM outperforms the Swin-L baseline (76.54% vs. 76.20%). For DeiT3, BHCCM brings mIoU gains of 0.53%, 0.15%, and 0.10% for DeiT3-B, 0.56%, 0.53%, and 0.35% for DeiT3-L.

Table III presents the results of Sentinel-2 imagery from the MM-5B. Compared to GaoFen-2, Sentinel-2 has significantly lower spatial resolution, which leads to lower overall performance. Nevertheless, consistent performance gains are observed with the introduction of BHCCM across all models. For ConvNeXt-B, the mIoU scores are improved by 1.76%, 0.87%, and 0.48% at Levels 1, 2, and 3, respectively. For DeiT3-B and DeiT3-L, the mIoU gains after applying BHCCM are (0.41%, 0.96%, 0.47%) and (0.55%, 0.82%, 0.91%), respectively.

Table IV summarizes the experimental results using Google imagery. Owing to its high spatial resolution, Google Earth imagery captures more detailed land cover characteristics, which increases intra-class variability and poses greater challenges for accurate interpretation. Nevertheless, both ConvNeXt-B and DeiT3, when enhanced with BHCCM, achieve consistent improvements over their baseline versions at all three hierarchical levels. Specifically, ConvNeXt-B achieves mIoU improvements of 3.26%, 3.44%, and 2.59%, while DeiT3-B yields gains of 3.86%, 2.51%, and 1.38%,

TABLE II

PERFORMANCE COMPARISON ON THE GAOFEN-2 SOURCE OF MM-5B DATASET. MODELS WITH BHCCM ARE MARKED AS (HIERA). OPTIMAL VALUES ARE HIGHLIGHTED IN RED, AND SUB-OPTIMAL VALUES ARE HIGHLIGHTED IN BLUE. EACH BACKBONE IS ANNOTATED ONLY ONCE.

Method	Backbone	Decode Head	L3 level		L2 level		L1 level	
			mIoU	mAcc	mIoU	mAcc	mIoU	mAcc
DeepLabv3+ [44]	ResNet-101 [51]	DSASPP [44]	70.59	81.79	81.22	87.61	93.16	96.04
DeepLabv3+ (Hiera)	ResNet-101	DSASPP + BHCCM	72.39	82.33	82.33	88.04	93.67	96.19
Segnext [52]	MSCA-S [52]	LightHam [52]	74.29	82.38	82.32	88.12	94.39	97.30
Segnext	MSCA-B [52]		74.74	82.69	83.37	89.23	94.59	97.33
Segnext	MSCA-L [52]		76.23	84.13	83.82	89.32	94.85	97.47
Segnext (Hiera)	MSCA-S	LightHam + BHCCM	74.77	82.60	83.57	88.23	94.53	97.32
Segnext (Hiera)	MSCA-B		75.72	83.57	83.63	89.22	94.62	97.38
Segnext (Hiera)	MSCA-L		76.59	84.86	84.32	89.95	94.86	97.47
ConvNeXt [48]	ConvNext-B [48]	UperNet [43]	73.73	81.54	82.38	88.08	93.85	96.78
ConvNext	ConvNext-L [48]		75.91	83.24	83.80	89.24	94.57	97.06
ConvNeXt (Hiera)	ConvNext-B	UperNet + BHCCM	74.77	82.63	83.35	89.18	94.39	97.33
ConvNeXt (Hiera)	ConvNext-L		75.83	83.15	83.66	89.20	94.55	97.06
Swin [54]	Swin-B [54]	UperNet	75.71	84.14	83.94	89.68	94.65	97.32
Swin	Swin-L		76.20	84.18	83.88	89.86	94.49	97.40
Swin (Hiera)	Swin-B	UperNet + BHCCM	76.54	84.87	84.60	90.43	94.85	97.43
Swin (Hiera)	Swin-L		76.66	84.93	84.66	90.50	94.88	97.48
DeiT III [53]	DeiT III-S [53]	UperNet	72.78	80.97	81.88	87.66	93.99	96.92
DeiT III	DeiT III-B [53]		73.45	81.53	82.55	88.22	94.13	97.06
DeiT III	DeiT III-L [53]		76.02	83.55	83.73	88.90	94.53	97.20
DeiT III (Hiera)	DeiT III-S	UperNet + BHCCM	73.04	81.23	81.93	87.82	94.01	96.92
DeiT III (Hiera)	DeiT III-B		73.98	81.81	82.70	88.28	94.23	97.11
DeiT III (Hiera)	DeiT III-L		76.58	83.69	84.26	89.57	94.91	97.45

TABLE III

PERFORMANCE COMPARISON ON THE SENTINEL-2 SOURCE OF MM-5B DATASET. MODELS WITH BHCCM ARE MARKED AS (HIERA). OPTIMAL VALUES ARE HIGHLIGHTED IN RED, AND SUB-OPTIMAL VALUES ARE HIGHLIGHTED IN BLUE. EACH BACKBONE IS ANNOTATED ONLY ONCE.

Method	Backbone	Decode Head	L3 level		L2 level		L1 level	
			mIoU	mAcc	mIoU	mAcc	mIoU	mAcc
ConvNeXt [48]	ConvNext-B [48]	UperNet [43]	61.00	70.05	71.16	79.86	82.58	88.92
ConvNext	ConvNext-L [48]		63.41	72.46	72.42	80.77	83.98	89.39
ConvNeXt (Hiera)	ConvNext-B	UperNet + BHCCM	62.76	71.54	72.03	80.55	83.06	89.06
ConvNeXt (Hiera)	ConvNext-L		63.54	72.52	72.56	80.85	84.26	89.58
DeiT III [53]	DeiT III-B [53]	UperNet	60.65	70.13	69.65	78.71	81.20	87.28
DeiT III	DeiT III-L [53]		61.61	71.34	71.26	80.34	82.35	88.56
DeiT III (Hiera)	DeiT III-B	UperNet + BHCCM	61.06	70.48	70.61	79.33	81.67	88.26
DeiT III (Hiera)	DeiT III-L		62.16	71.65	72.08	80.85	83.26	88.78

respectively.

2) *Qualitative Results*: Fig. 8 clearly demonstrates the performance improvements brought by the proposed BHCCM on GaoFen-2 data at the L3 level. In contrast, Fig. 9 illustrates the interpretation results at different spatial resolutions and highlights the strict semantic consistency across hierarchical levels for the GaoFen-2, Sentinel-2, and Google Earth data sources.

D. Transfer LCLU Classification Model to Crop Classification

To evaluate the effectiveness of the proposed TransLU framework, we assess its transferability in crop classification scenarios using the Crop10m dataset. This experiment is designed to examine the generalization and scalability of TransLU in real-world applications. Specifically, a hierarchical

LCLU classification model trained on Sentinel-2 data from the MM-5B dataset is transferred to Crop10m dataset, enabling the expansion of crop categories while preserving the model's capacity for hierarchical LCLU classification.

1) *Quantitative Results*: Table V presents the results of transferring the hierarchical LCLU classification models based on ConvNeXt and DeiT3 (representing CNN and Transformer architectures, respectively) to the crop classification task using the proposed TransLU framework. The hierarchical LCLU models used for transfer are based on ConvNeXt-B and DeiT3-B, as reported in Table III.

By comparing the conventional baseline methods with our proposed dual-branch TransLU, it is evident that TransLU effectively enhances performance in in cross-domain scenarios. Specifically, for ConvNeXt-B, the mIoU improves

TABLE IV
PERFORMANCE COMPARISON ON THE GOOGLE EARTH SOURCE OF MM-5B DATASET. MODELS WITH BHCCM ARE MARKED AS (HIERA). OPTIMAL VALUES ARE HIGHLIGHTED IN RED, AND SUB-OPTIMAL VALUES ARE HIGHLIGHTED IN BLUE. EACH BACKBONE IS ANNOTATED ONLY ONCE.

Method	Backbone	Decode Head	L3 level		L2 level		L1 level	
			mIoU	mAcc	mIoU	mAcc	mIoU	mAcc
ConvNeXt [48]	ConvNext-B [48]	UperNet [43]	57.08	68.87	61.99	72.68	71.05	79.81
ConvNeXt (Hiera)	ConvNext-B	UperNet + BHCCM	60.34	70.23	65.43	75.63	73.64	83.62
DeiT III [53]	Deit III-B [53]	UperNet	57.47	69.48	63.15	74.09	71.25	80.37
DeiT III (Hiera)	Deit III-B	UperNet + BHCCM	61.33	71.45	65.66	76.03	75.02	85.23

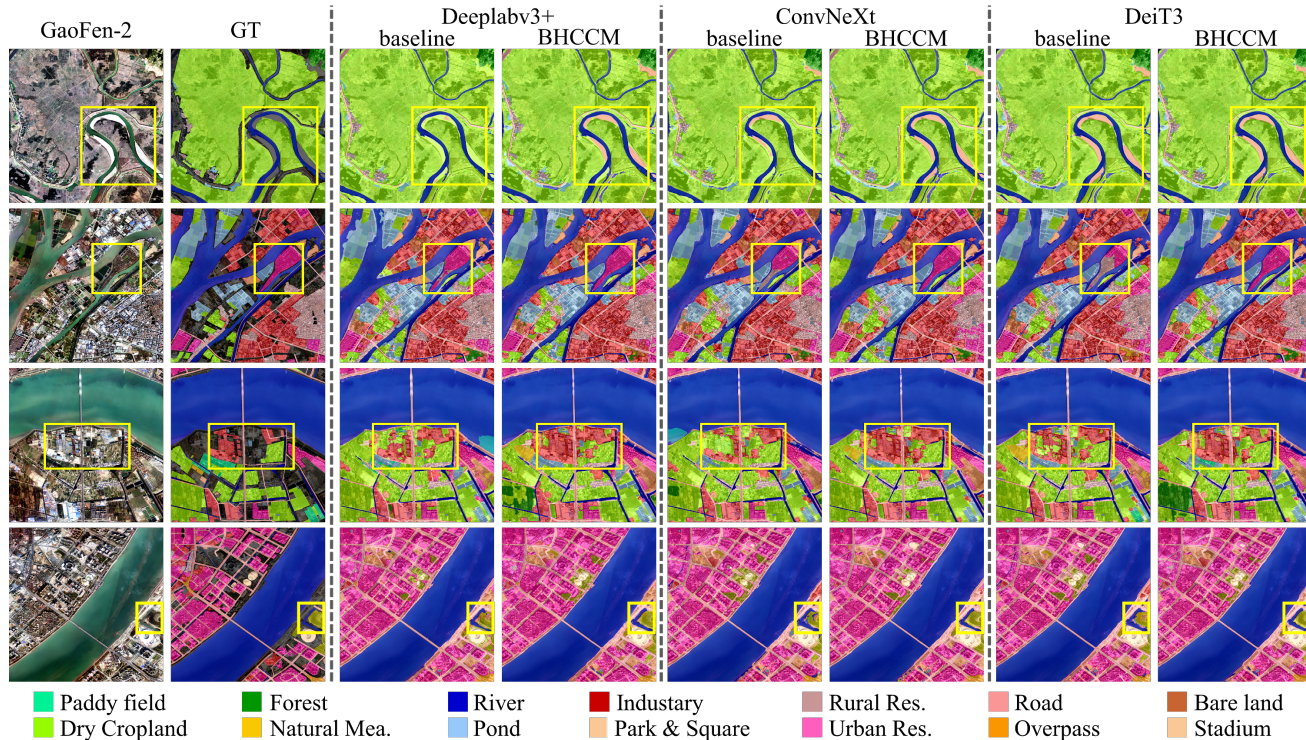


Fig. 8. Visualization results on the GaoFen-2 modality of the MM-5B dataset. The figure demonstrates the performance improvements at the finest level (L3) achieved by the proposed BHCCM method.

by 2.07%, with class-wise increases of 0.77% for rice, 0.48% for corn, 2.21% for soybean, and 5.82% for the “other” class. The substantial gain in the “other” class strongly demonstrates that TransLU can effectively help the crop classification model improve its ability to distinguish easily confused land cover types. Similarly, for the DeiT3-B model, TransLU yields an mIoU improvement of 1.51%, with corresponding class-wise gains of 1.08%, 1.59%, 1.70%, and 1.63% across the four categories.

2) *Qualitative Results*: The proposed TransLU model not only enables the transfer of hierarchical LCLU models across different architectures, but also demonstrates strong potential for new category expansion. It allows crop classification tasks to be interpreted as a fine-grained extension of hierarchical LCLU classification, by dynamically expanding the tree-structured hierarchy based on application needs. As illustrated in Fig. 3 (d), crop classification can be regarded as a

further subdivision of the cultivated land category at the L3 or L4 levels. Similarly, TransLU is capable of supporting other hierarchical refinements, such as “*Artificial Surfaces* → *Industrial Area* → *Storage Tanks*”, or “*Artificial Surfaces* → *Transportation* → *Roads* → *Highway*”. Fig. 10 visualizes the LCLU classification results when treating crop classification as an extension of LCLU classification, where cropland is further divided into rice, corn, and soybeans at the L3 level.

E. Transfer LCLU Classification Models Across Heterogeneous Classification Systems

Table VI presents the results of transferring a pretrained hierarchical LCLU model to a heterogeneous classification system using the proposed TransLU framework. Specifically, the hierarchical LCLU model in Branch2 was trained on the Google Earth imagery subset from the MM-5B dataset. The experimental results indicate that applying the TransLU

TABLE V
CROP CLASSIFICATION PERFORMANCE COMPARISON ON THE CROP10M DATASET. THE BEST PERFORMANCE IS SHOWN IN **BOLD**.

Model	Method	Branch1		Branch2		Crop10m Crop Classification				
		Encoder	Decoder	Encoder	Decoder	mIoU	Rice	Corn	Soybean	Others
ConvNext [48]	baseline	ConvNext-B	UperNet	—	—	78.25	86.37	78.52	69.53	78.56
	TransLU	ConvNext-B	UperNet+BHCCM	ConvNext-B	UperNet+BHCCM	80.32	87.14	79.00	70.74	84.38
DeiT3 [53]	baseline	DeiT3-B	UperNet	—	—	76.92	86.48	76.20	67.50	77.52
	TransLU	DeiT3-B	UperNet+BHCCM	DeiT3-B	UperNet+BHCCM	78.43	87.56	77.79	69.20	79.15

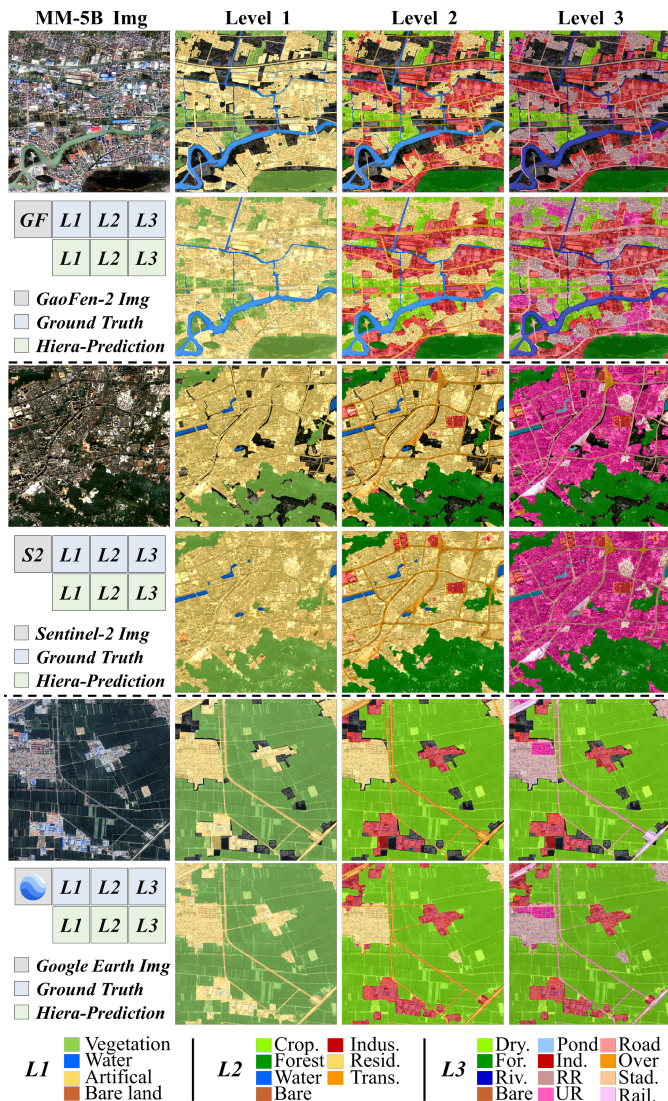


Fig. 9. Hierarchical LCLU classification results of ConvNeXt-B combined with the proposed BHCCM across the three data sources in the MM-5B dataset. The figure shows the interpretation results under different modalities, as well as the strict consistency of hierarchical predictions across the L1-L2-L3 levels within each individual source.

framework to transfer the hierarchical LCLU model to a task with a different label hierarchy significantly improves performance compared with the baseline. For ConvNeXt-B, mIoU increases by 3.11% and mAcc by 3.18%. For DeiT-B, mIoU improves by 2.71% and mAcc by 2.36%.

These findings demonstrate that TransLU is highly

TABLE VI
PERFORMANCE COMPARISON ON THE WHDL D DATASET. THE BEST PERFORMANCE IS SHOWN IN **BOLD**.

Model	Method	mIoU	mAcc
ConvNext-B [48]	baseline	65.10	76.45
	TransLU	68.21	79.63
DeiT3-B [53]	baseline	64.36	75.67
	TransLU	67.34	78.03

adaptable across different network architectures and that transferring a pretrained hierarchical LCLU model can outperform training a new model from scratch. This suggests a promising paradigm for efficiently adapting well-trained hierarchical LCLU models to other domains. The visualization in Fig. 11 compares the ConvNeXt-B model under the baseline and TransLU frameworks, intuitively highlighting the effectiveness of our method in improving classification accuracy.

F. Ablation Study

1) **BHCCM**: In the ablation study of BHCCM, we validate the effectiveness of its internal design of bidirectional semantic consistency constraints as well as the proposed loss function \mathcal{L}_{HSC} . As shown in Table VII, we use ConvNeXt-Base with a flat classification structure as the baseline, which achieves an mIoU of 73.73% and an mAcc of 80.06% on the GaoFen-2 data of MM-5B dataset. We design five comparative settings:

(1) **Without fusion** (\mathcal{L}_{HCE}): mIoU = 71.36%, using three independent 2D convolutions generated the final results, led to a significant performance drop, decreasing by 2.37% compared to the baseline.

(2) **Coarse-to-fine** (\mathcal{L}_{HCE}): mIoU = 72.57%, improves by 1.21% compared to setting 1), but still falls short of the baseline by 1.16%.

(3) **Fine-to-coarse** (\mathcal{L}_{HCE}): mIoU = 72.55%, which is still 1.18% lower than the baseline.

(4) **Bidirectional** (\mathcal{L}_{HCE}): mIoU = 73.75%, improved performance by 2.39% compared to the 1) setting, essentially restoring it to baseline levels.

(5) **Bidirectional** (\mathcal{L}_{HSC}): mIoU = 74.77%. Finally, on top of the bidirectional information fusion, we integrated the proposed hierarchical semantic consistency constraint \mathcal{L}_{HSC} . Under this setting, the mIoU reached 74.77%, and the mAcc improved to 81.15%, showing improvements of 1.04% and 1.09% over the baseline, respectively.

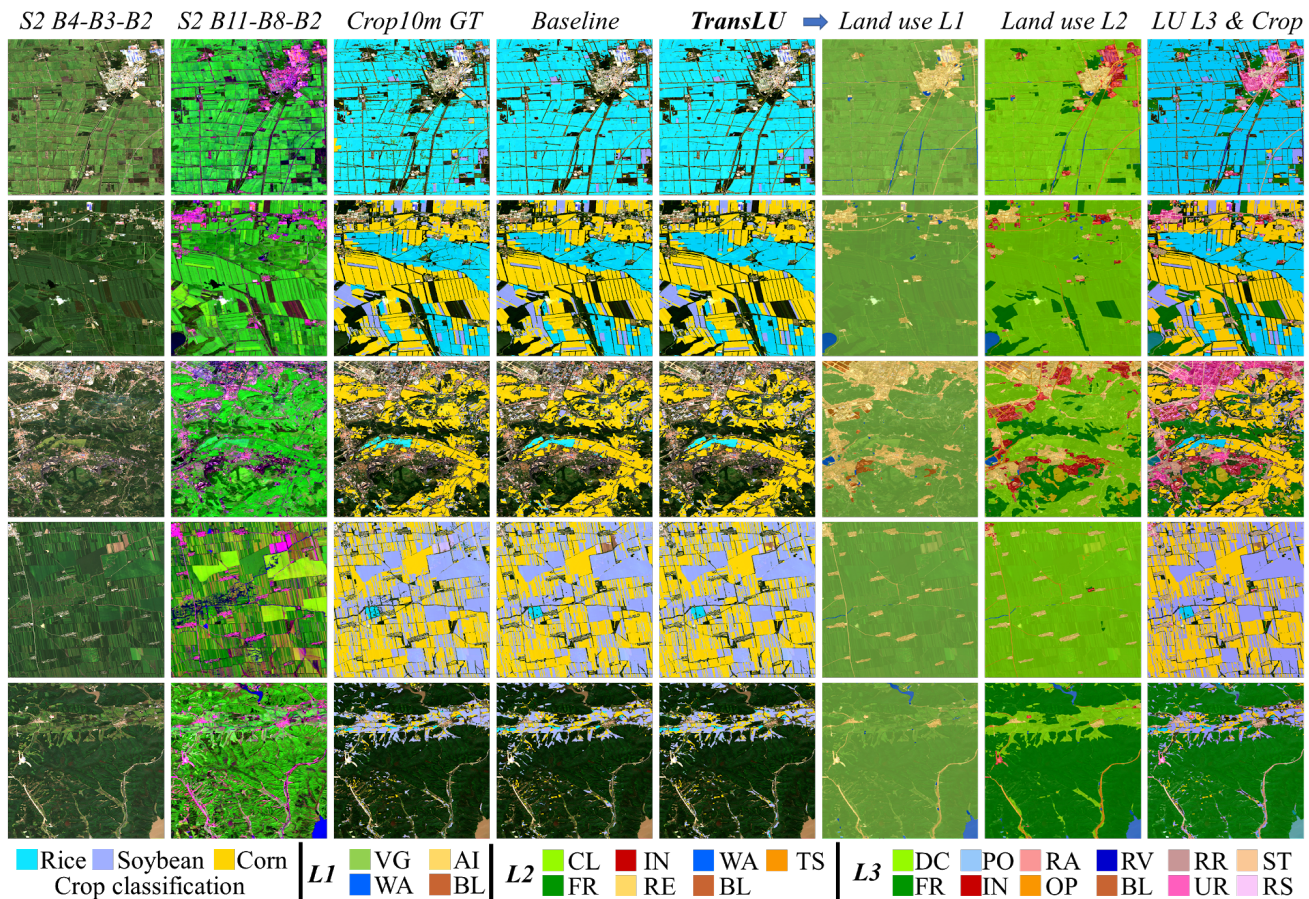


Fig. 10. Visualization of crop classification results on the Crop10m dataset. This figure presents the results of transferring the hierarchical LCLU classification model (ConvNeXt-B + BHCCM) to crop classification. The first two columns show Sentinel-2 images with different band combinations, highlighting the importance of spectral features for crop identification. *Baseline* refers to the flat ConvNeXt-B model trained from scratch, while *TransLU* denotes the results using the proposed dual-branch transfer framework. *Land use L1* and *Land use L2* represent the L1 and L2 level land use classification results inferred from Branch 2 in TransLU. The last column displays the final prediction by fusing the L3 land use outputs with the crop classification from Branch 1, demonstrating the effectiveness of TransLU in cross-domain transfer tasks.

TABLE VII
ABLATION ANALYSIS OF BHCCM AND \mathcal{L}_{HSC} . VALUES LOWER THAN THE BASELINE ARE HIGHLIGHTED IN BLUE, WHILE THOSE HIGHER ARE HIGHLIGHTED IN RED.

ID	Method	Loss F.	mIoU
0	Baseline	\mathcal{L}_{CE}	73.73
1	+ BHCCM (without fusin)	\mathcal{L}_{HCE}	71.36 (-2.37%)
2	+ BHCCM (coarse-to-fine)	\mathcal{L}_{HCE}	72.57 (-1.16%)
3	+ BHCCM (fine-to-coarse)	\mathcal{L}_{HCE}	72.55 (-1.18%)
4	+ BHCCM (bidirectional)	\mathcal{L}_{HCE}	73.75 (+0.02%)
5	+ BHCCM (bidirectional)	\mathcal{L}_{HSC}	74.77 (+1.04%)

These results clearly demonstrate that the bidirectional semantic consistency constraints and the hierarchical semantic consistency loss in BHCCM significantly enhance the performance of hierarchical LCLU classification.

2) *CDKS and CDSA*: The proposed TransLU framework consists of two key components—CDKS and CDSA. To evaluate their effectiveness, we conducted ablation studies on the Crop10m crop classification task. The baseline is defined as a model trained from scratch without using TransLU.

Table VIII presents the ablation results of CDKS in the TransLU framework, where both branches use the same model architecture. When CDKS is not applied, replacing the ImageNet-pretrained weights in Branch 1 with weights trained on the MM-5B dataset leads to a modest performance improvement. Specifically, mIoU improves by 0.43% for ConvNeXt and 0.51% for DeiT. This outcome aligned with our expectations, as models pre-trained on the MM-5B dataset are already adapted to the characteristics of Sentinel-2 imagery, thus offering a performance advantage over those initialized with generic ImageNet weights. Furthermore, when integrate CDKS into TransLU, we observed a significant performance improvement. For ConvNeXt-B, the use of CDKS leads to an increase of 1.15% for mIoU and 0.6% for mAcc compared to the baseline. For DeiT-B, the improvements over the baseline were 1.1% for mIoU and 0.69% for mAcc, respectively. This validates the effectiveness of our proposed CDKS.

Furthermore, we conducted ablation experiments to evaluate the proposed CDSA. We compared the model performance differences before and after applying CDSA. As shown in Table IX, a clear performance improvement was observed when TransLU is equipped with CDSA. Specifically, for

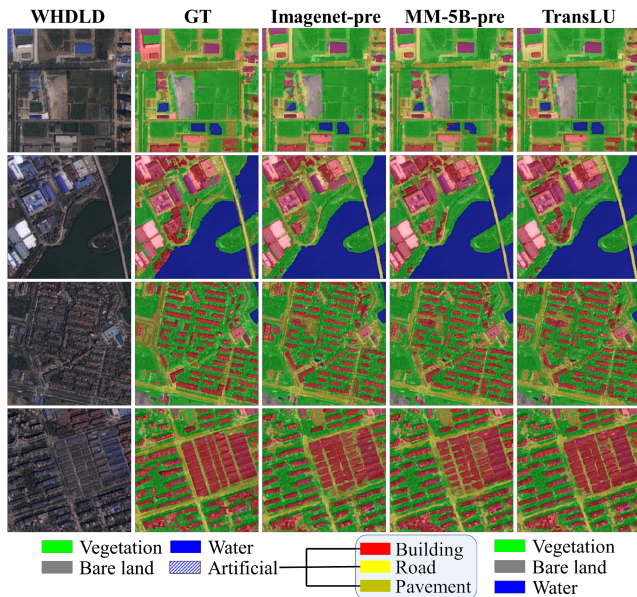


Fig. 11. Visualization of LCLU classification results on the WHDL D dataset. The figure presents the classification results of the ConvNeXt model under three settings: 1) trained from scratch with ImageNet pre-trained weights, 2) trained from scratch with MM-5B pre-trained weights, and 3) the hierarchical model (ConvNeXt + BHCCM) transferred via the TransLU framework. The bottom part of the figure illustrates the tree-structured hierarchy used in TransLU.

TABLE VIII
ABLATION ANALYSIS OF CDKS. OPTIMAL VALUES ARE HIGHLIGHTED IN RED, AND SUB-OPTIMAL VALUES ARE HIGHLIGHTED IN BLUE.

Model	Branch1 Pre.	CDKS	mIoU	mAcc
ConvNeXt [48]	ImageNet-21k	No	78.25	87.67
	MM-5B (S2)	No	78.68	88.02
Yes		79.40	88.27	
DeiT3 [53]	ImageNet-21k	No	76.92	86.67
	MM-5B (S2)	No	77.43	86.95
Yes		78.02	87.36	

ConvNeXt-B, incorporating CDSA leads to increases of 0.91% in mIoU and 0.48% in mAcc, compared to the baseline without CDSA. Similarly, for DeiT3-B, CDSA improves mIoU and mAcc by 0.41% and 0.86%, respectively. These results provide strong evidence for the effectiveness of the proposed CDSA in facilitating LCLU model transfer for cross-domain EO tasks.

3) *JSPS Post-processing Strategy*: We validate the effectiveness of the proposed joint score-based path selection strategy on the GaoFen-2 modality within the MM-5B dataset. As summarized in Table X, applying this post-processing method during inference not only enforces strict compliance with the predefined tree-structured hierarchy for multi-granularity outputs, but also yields marginal improvements in classification performance. Although the gains are minor, they demonstrate that BHCCM inherently provides strong consistency in hierarchical predictions, even without explicit post-processing.

TABLE IX
ABLATION ANALYSIS OF CDSA. THE BEST PERFORMANCE IS SHOWN IN BOLD.

Model	CDKS	CDSA	mIoU	mAcc
ConvNeXt-B [48]	Yes	No	79.40	88.27
		Yes	80.32	88.75
DeiT3-B [53]	Yes	No	78.02	87.36
		Yes	78.43	88.22

TABLE X
ABLATION ANALYSIS OF JSPS POST-PROCESS STRATEGY. THE BEST PERFORMANCE IS SHOWN IN BOLD.

Model	Post-pro	L3	L2	L1
ConvNeXt-B [48]	No	74.71	83.30	94.33
	Yes	74.77	83.35	94.39

VI. CONCLUSION

This paper addresses two critical challenges in hierarchical LCLU classification and cross-domain task transfer by introducing HierRS, a novel hierarchical interpretation paradigm. To enable multi-granularity and semantically consistent hierarchical LCLU classification, we propose the BHCCM, which embeds the inherent tree-structured relationships of land categories as semantic constraints within the model. This allows for transforming conventional flat classification models into hierarchical models with consistent predictions across levels, while also improving classification accuracy at each level. To enhance the transferability of LCLU models to cross-domain EO tasks, we propose TransLU, a dual-branch framework designed for cross-domain adaptation. With two key components—CDKS and CDSA, TransLU enables category expansion and efficient adaptation of LCLU models to EO tasks with heterogeneous hierarchical classification systems, promoting strong generalization and reducing reliance on labeled data in target domains. Additionally, we introduce \mathcal{L}_{HSC} to enforce semantic consistency during training. Furthermore, we contribute MM-5B to the RS community, a large-scale multi-modal hierarchical land use dataset with pixel-level annotated. MM-5B includes imagery from three types of sensors, covering diverse spatial resolutions and spectral characteristics. Extensive experiments on MM-5B, Crop10m, and WHDL D demonstrate that the proposed HierRS hierarchical interpretation paradigm achieves outstanding performance in both multi-granularity hierarchical LCLU classification and cross-domain transfer tasks.

In future work, we plan to further explore the adaptability of HierRS to multi-modal methods. Leveraging the rich spectral diversity and spatial resolution settings of the MM-5B dataset, we aim to develop more effective multi-modal hierarchical interpretation techniques to improve the practicality of RS-based Earth Observation.

REFERENCES

- [1] B. Wu, M. Zhang, H. Zeng, F. Tian, A. B. Potgieter, X. Qin, N. Yan, S. Chang, Y. Zhao, Q. Dong *et al.*, “Challenges and opportunities in remote sensing-based crop monitoring: A review,” *National Science Review*, vol. 10, no. 4, p. nwac290, 2023.
- [2] Q. Yuan, H. Shen, T. Li, Z. Li, S. Li, Y. Jiang, H. Xu, W. Tan, Q. Yang, J. Wang *et al.*, “Deep learning in environmental remote sensing: Achievements and challenges,” *Remote sensing of Environment*, vol. 241, p. 111716, 2020.
- [3] X.-Y. Tong, G.-S. Xia, and X. X. Zhu, “Enabling country-scale land cover mapping with meter-resolution satellite imagery,” *ISPRS Journal of Photogrammetry and Remote Sensing*, vol. 196, pp. 178–196, 2023. [Online]. Available: <https://www.sciencedirect.com/science/article/pii/S0924271622003264>
- [4] X. Zhang, T. Zhao, H. Xu, W. Liu, J. Wang, X. Chen, and L. Liu, “Glc_fcs30d: The first global 30-m land-cover dynamic monitoring product with a fine classification system from 1985 to 2022 using dense time-series landsat imagery and continuous change-detection method,” *Earth System Science Data Discussions*, vol. 2023, pp. 1–32, 2023.
- [5] D. Hong, B. Zhang, H. Li, Y. Li, J. Yao, C. Li, M. Werner, J. Chanussot, A. Zipf, and X. X. Zhu, “Cross-city matters: A multimodal remote sensing benchmark dataset for cross-city semantic segmentation using high-resolution domain adaptation networks,” *Remote Sensing of Environment*, vol. 299, p. 113856, 2023. [Online]. Available: <https://www.sciencedirect.com/science/article/pii/S0034425723004078>
- [6] R. Liu, J. Ling, and H. Zhang, “Softformer: Sar-optical fusion transformer for urban land use and land cover classification,” *ISPRS Journal of Photogrammetry and Remote Sensing*, vol. 218, pp. 277–293, 2024.
- [7] Z. Xue, X. Yu, A. Yu, B. Liu, P. Zhang, and S. Wu, “Self-supervised feature learning for multimodal remote sensing image land cover classification,” *IEEE Transactions on Geoscience and Remote Sensing*, vol. 60, pp. 1–15, 2022.
- [8] W. Kang, Y. Xiang, F. Wang, and H. You, “Cfnets: A cross fusion network for joint land cover classification using optical and sar images,” *IEEE Journal of Selected Topics in Applied Earth Observations and Remote Sensing*, vol. 15, pp. 1562–1574, 2022.
- [9] C. Zhang, I. Sargent, X. Pan, H. Li, A. Gardiner, J. Hare, and P. M. Atkinson, “Joint deep learning for land cover and land use classification,” *Remote sensing of environment*, vol. 221, pp. 173–187, 2019.
- [10] C. Yang, F. Rottensteiner, and C. Heipke, “Exploring semantic relationships for hierarchical land use classification based on convolutional neural networks,” *ISPRS Annals of the Photogrammetry, Remote Sensing and Spatial Information Sciences*, vol. 2, pp. 599–607, 2020.
- [11] L. Liu, Z. Tong, Z. Cai, H. Wu, R. Zhang, A. Le Bris, and A.-M. Olteanu-Raimond, “Hieru-net: A hierarchical semantic segmentation method for land cover mapping,” *IEEE Transactions on Geoscience and Remote Sensing*, 2024.
- [12] X. Kang, Y. Hong, P. Duan, and S. Li, “Fusion of hierarchical class graphs for remote sensing semantic segmentation,” *Information Fusion*, vol. 109, p. 102409, 2024.
- [13] X. Guo, J. Lao, B. Dang, Y. Zhang, L. Yu, L. Ru, L. Zhong, Z. Huang, K. Wu, D. Hu, H. He, J. Wang, J. Chen, M. Yang, Y. Zhang, and Y. Li, “Skysense: A multi-modal remote sensing foundation model towards universal interpretation for earth observation imagery,” in *2024 IEEE/CVF Conference on Computer Vision and Pattern Recognition (CVPR)*, 2024, pp. 27 662–27 673.
- [14] X. Sun, P. Wang, W. Lu, Z. Zhu, X. Lu, Q. He, J. Li, X. Rong, Z. Yang, H. Chang, Q. He, G. Yang, R. Wang, J. Lu, and K. Fu, “Ringmo: A remote sensing foundation model with masked image modeling,” *IEEE Transactions on Geoscience and Remote Sensing*, vol. 61, pp. 1–22, 2023.
- [15] D. Wang, M. Hu, Y. Jin, Y. Miao, J. Yang, Y. Xu, X. Qin, J. Ma, L. Sun, C. Li, C. Fu, H. Chen, C. Han, N. Yokoya, J. Zhang, M. Xu, L. Liu, L. Zhang, C. Wu, B. Du, D. Tao, and L. Zhang, “Hypersigma: Hyperspectral intelligence comprehension foundation model,” *IEEE Transactions on Pattern Analysis and Machine Intelligence*, pp. 1–18, 2025.
- [16] J. Wang, A. Ma, Y. Zhong, Z. Zheng, and L. Zhang, “Cross-sensor domain adaptation for high spatial resolution urban land-cover mapping: From airborne to spaceborne imagery,” *Remote Sensing of Environment*, vol. 277, p. 113058, 2022.
- [17] M. Luo and S. Ji, “Cross-spatiotemporal land-cover classification from vhr remote sensing images with deep learning based domain adaptation,” *ISPRS Journal of Photogrammetry and Remote Sensing*, vol. 191, pp. 105–128, 2022.
- [18] M. Martini, V. Mazzia, A. Khaliq, and M. Chiaberge, “Domain-adversarial training of self-attention-based networks for land cover classification using multi-temporal sentinel-2 satellite imagery,” *Remote Sensing*, vol. 13, no. 13, p. 2564, 2021.
- [19] Q. Li, Y. Wen, J. Zheng, Y. Zhang, and H. Fu, “Hyunida: Breaking label set constraints for universal domain adaptation in cross-scene hyperspectral image classification,” *IEEE Transactions on Geoscience and Remote Sensing*, 2024.
- [20] Y. Meng, Z. Yuan, J. Yang, P. Liu, J. Yan, H. Zhu, Z. Ma, Z. Jiang, Z. Zhang, and X. Mi, “Cross-domain land cover classification of remote sensing images based on full-level domain adaptation,” *IEEE Journal of Selected Topics in Applied Earth Observations and Remote Sensing*, 2024.
- [21] J. Wang, Z. Zheng, A. Ma, X. Lu, and Y. Zhong, “Loveda: A remote sensing land-cover dataset for domain adaptive semantic segmentation,” *arXiv preprint arXiv:2110.08733*, 2021.
- [22] Z. Shao, K. Yang, and W. Zhou, “Performance evaluation of single-label and multi-label remote sensing image retrieval using a dense labeling dataset,” *Remote Sensing*, vol. 10, no. 6, p. 964, 2018.
- [23] I. Demir, K. Koperski, D. Lindenbaum, G. Pang, J. Huang, S. Basu, F. Hughes, D. Tuia, and R. Raskar, “Deepglobe 2018: A challenge to parse the earth through satellite images,” in *Proceedings of the IEEE conference on computer vision and pattern recognition workshops*, 2018, pp. 172–181.
- [24] C. Robinson, L. Hou, K. Malkin, R. Soobitsky, J. Czawlytko, B. Dilkina, and N. Jovic, “Large scale high-resolution land cover mapping with multi-resolution data,” in *Proceedings of the IEEE/CVF Conference on Computer Vision and Pattern Recognition*, 2019, pp. 12 726–12 735.
- [25] J. Li, X. Huang, and L. Tu, “Whu-ohs: A benchmark dataset for large-scale herseprtral image classification,” *International Journal of Applied Earth Observation and Geoinformation*, vol. 113, p. 103022, 2022.
- [26] M. Schmitt, L. Hughes, C. Qiu, and X. Zhu, “Sen12ms—a curated dataset of georeferenced multi-spectral sentinel-1/2 imagery for deep learning and data fusion. arxiv 2019,” *arXiv preprint arXiv:1906.07789*, 2019.
- [27] C. Robinson, K. Malkin, N. Jovic, H. Chen, R. Qin, C. Xiao, M. Schmitt, P. Ghamisi, R. Hänsch, and N. Yokoya, “Global land-cover mapping with weak supervision: Outcome of the 2020 ieeec grss data fusion contest,” *IEEE Journal of Selected Topics in Applied Earth Observations and Remote Sensing*, vol. 14, pp. 3185–3199, 2021.
- [28] Z. Xiong, S. Chen, Y. Wang, L. Mou, and X. X. Zhu, “Gamus: A geometry-aware multi-modal semantic segmentation benchmark for remote sensing data,” *arXiv preprint arXiv:2305.14914*, 2023.
- [29] C. Robinson, L. Hou, K. Malkin, R. Soobitsky, J. Czawlytko, B. Dilkina, and N. Jovic, “Large scale high-resolution land cover mapping with multi-resolution data,” in *Proceedings of the IEEE/CVF Conference on Computer Vision and Pattern Recognition*, 2019, pp. 12 726–12 735.
- [30] —, “Large scale high-resolution land cover mapping with multi-resolution data,” in *Proceedings of the IEEE/CVF Conference on Computer Vision and Pattern Recognition*, 2019, pp. 12 726–12 735.
- [31] N. Johnson, W. Treible, and D. Crispell, “Opensentinelmap: A large-scale land use dataset using opentstreetmap and sentinel-2 imagery,” in *Proceedings of the IEEE/CVF Conference on Computer Vision and Pattern Recognition*, 2022, pp. 1333–1341.
- [32] S. Talukdar, P. Singha, S. Mahato, S. Pal, Y.-A. Liou, and A. Rahman, “Land-use land-cover classification by machine learning classifiers for satellite observations—a review,” *Remote sensing*, vol. 12, no. 7, p. 1135, 2020.
- [33] Z. Li, B. Chen, S. Wu, M. Su, J. M. Chen, and B. Xu, “Deep learning for urban land use category classification: A review and experimental assessment,” *Remote Sensing of Environment*, vol. 311, p. 114290, 2024.
- [34] N. Kussul, M. Lavreniuk, S. Skakun, and A. Shelestov, “Deep learning classification of land cover and crop types using remote sensing data,” *IEEE Geoscience and Remote Sensing Letters*, vol. 14, no. 5, pp. 778–782, 2017.
- [35] R. Liu, J. Ling, and H. Zhang, “Softformer: Sar-optical fusion transformer for urban land use and land cover classification,” *ISPRS Journal of Photogrammetry and Remote Sensing*, vol. 218, pp. 277–293, 2024.
- [36] Z. Gong, Z. Wei, D. Wang, X. Ma, H. Chen, Y. Jia, Y. Deng, Z. Ji, X. Zhu, N. Yokoya *et al.*, “Crossearch: Geospatial vision foundation model for domain generalizable remote sensing semantic segmentation,” *arXiv preprint arXiv:2410.22629*, 2024.
- [37] R. Dong, L. Mou, M. Chen, W. Li, X.-Y. Tong, S. Yuan, L. Zhang, J. Zheng, X. Zhu, and H. Fu, “Large-scale land cover mapping with fine-

- grained classes via class-aware semi-supervised semantic segmentation,” in *Proceedings of the IEEE/CVF International Conference on Computer Vision*, 2023, pp. 16 783–16 793.
- [38] Z. Li, W. He, M. Cheng, J. Hu, G. Yang, and H. Zhang, “Sinolc-1: The first 1-meter resolution national-scale land-cover map of china created with the deep learning framework and open-access data,” *Earth System Science Data Discussions*, vol. 2023, pp. 1–38, 2023.
- [39] A. Waśniewski, A. Hościło, and M. Chmielewska, “Can a hierarchical classification of sentinel-2 data improve land cover mapping?” *Remote Sensing*, vol. 14, no. 4, p. 989, 2022.
- [40] C. Yang, F. Rottensteiner, and C. Heipke, “A hierarchical deep learning framework for the consistent classification of land use objects in geospatial databases,” *ISPRS Journal of Photogrammetry and Remote Sensing*, vol. 177, pp. 38–56, 2021.
- [41] L. Li, W. Wang, T. Zhou, R. Quan, and Y. Yang, “Semantic hierarchy-aware segmentation,” *IEEE Transactions on Pattern Analysis and Machine Intelligence*, vol. 46, no. 4, pp. 2123–2138, 2023.
- [42] L. Liu, S. Wang, Z. Tong, and Z. Cai, “Clustering-based class hierarchy modeling for semantic segmentation using remotely sensed imagery,” *Mathematics*, vol. 13, no. 3, p. 331, 2025.
- [43] T. Xiao, Y. Liu, B. Zhou, Y. Jiang, and J. Sun, “Unified perceptual parsing for scene understanding,” in *Proceedings of the European Conference on Computer Vision (ECCV)*, September 2018.
- [44] L.-C. Chen, Y. Zhu, G. Papandreou, F. Schroff, and H. Adam, “Encoder-decoder with atrous separable convolution for semantic image segmentation,” in *Proceedings of the European Conference on Computer Vision (ECCV)*, September 2018.
- [45] X. Zhu, X. Yang, Z. Wang, H. Li, W. Dou, J. Ge, L. Lu, Y. Qiao, and J. Dai, “Parameter-inverted image pyramid networks,” in *Advances in Neural Information Processing Systems*, A. Globerson, L. Mackey, D. Belgrave, A. Fan, U. Paquet, J. Tomczak, and C. Zhang, Eds., vol. 37. Curran Associates, Inc., 2024, pp. 132 267–132 288. [Online]. Available: https://proceedings.neurips.cc/paper_files/paper/2024/file/ee81a23d6b83ac15fb5b7a30934e0b-Paper-Conference.pdf
- [46] X. Zhu, W. Su, L. Lu, B. Li, X. Wang, and J. Dai, “Deformable detr: Deformable transformers for end-to-end object detection,” *arXiv preprint arXiv:2010.04159*, 2020.
- [47] J. L. Ba, J. R. Kiros, and G. E. Hinton, “Layer normalization,” *arXiv preprint arXiv:1607.06450*, 2016.
- [48] Z. Liu, H. Mao, C.-Y. Wu, C. Feichtenhofer, T. Darrell, and S. Xie, “A convnet for the 2020s,” *Proceedings of the IEEE/CVF Conference on Computer Vision and Pattern Recognition (CVPR)*, 2022.
- [49] A. Dosovitskiy, L. Beyer, A. Kolesnikov, D. Weissenborn, X. Zhai, T. Unterthiner, M. Dehghani, M. Minderer, G. Heigold, S. Gelly, J. Uszkoreit, and N. Houlsby, “An image is worth 16x16 words: Transformers for image recognition at scale,” 2021. [Online]. Available: <https://arxiv.org/abs/2010.11929>
- [50] N. You, J. Dong, J. Huang, G. Du, G. Zhang, Y. He, T. Yang, Y. Di, and X. Xiao, “The 10-m crop type maps in northeast china during 2017–2019,” *Scientific data*, vol. 8, no. 1, p. 41, 2021.
- [51] K. He, X. Zhang, S. Ren, and J. Sun, “Deep residual learning for image recognition,” in *Proceedings of the IEEE Conference on Computer Vision and Pattern Recognition (CVPR)*, June 2016.
- [52] M.-H. Guo, C.-Z. Lu, Q. Hou, Z. Liu, M.-M. Cheng, and S.-m. Hu, “Segnext: Rethinking convolutional attention design for semantic segmentation,” in *Advances in Neural Information Processing Systems*, S. Koyejo, S. Mohamed, A. Agarwal, D. Belgrave, K. Cho, and A. Oh, Eds., vol. 35. Curran Associates, Inc., 2022, pp. 1140–1156.
- [53] H. Touvron, M. Cord, and H. Jégou, “Deit iii: Revenge of the vit,” in *European conference on computer vision*. Springer, 2022, pp. 516–533.
- [54] Z. Liu, Y. Lin, Y. Cao, H. Hu, Y. Wei, Z. Zhang, S. Lin, and B. Guo, “Swin transformer: Hierarchical vision transformer using shifted windows,” in *2021 IEEE/CVF International Conference on Computer Vision (ICCV)*, 2021, pp. 9992–10 002.
- [55] M. Contributors, “MMSegmentation: Openmmlab semantic segmentation toolbox and benchmark,” <https://github.com/open-mmlab/mms Segmentation>, 2020.